


ORIGINAL ARTICLE

Open Access



# Radiologic-pathologic correlation in breast cancer: do MRI biomarkers correlate with pathologic features and molecular subtypes?

Francesca Galati, Veronica Rizzo\* , Giuliana Moffa, Claudia Caramanico, Endi Kripa, Bruna Cerbelli, Giulia D'Amati and Federica Pediconi

## Abstract

**Background:** Breast cancer (BC) includes different pathological and molecular subtypes. This study aimed to investigate whether multiparametric magnetic resonance imaging (mpMRI) could reliably predict the molecular status of BC, comparing mpMRI features with pathological and immunohistochemical results.

**Methods:** This retrospective study included 156 patients with an ultrasound-guided biopsy-proven BC, who underwent breast mpMRI (including diffusion-weighted imaging) on a 3-T scanner from 2017 to 2020. Histopathological analyses were performed on the surgical specimens. Kolmogorov–Smirnov  $Z$ ,  $\chi^2$ , and univariate and multivariate logistic regression analyses were performed.

**Results:** Fifteen patients were affected with ductal carcinoma *in situ*, 122 by invasive carcinoma of no special type, and 19 with invasive lobular carcinoma. Out of a total of 141 invasive cancers, 45 were luminal A-like, 54 luminal B-like, 5 human epidermal growth factor receptor 2 (HER2) positive, and 37 triple negative. The regression analyses showed that size < 2 cm predicted luminal A-like status ( $p = 0.025$ ), while rim enhancement ( $p < 0.001$ ), intralesional necrosis ( $p = 0.001$ ), peritumoural oedema ( $p < 0.001$ ), and axillary adenopathies ( $p = 0.012$ ) were negative predictors. Oppositely, round shape ( $p = 0.001$ ), rim enhancement ( $p < 0.001$ ), intralesional necrosis ( $p < 0.001$ ), and peritumoural oedema ( $p < 0.001$ ) predicted triple-negative status.

**Conclusions:** mpMRI has been confirmed to be a valid noninvasive predictor of BC subtypes, especially luminal A and triple negative. Considering the central role of pathology in BC diagnosis and immunohistochemical profiling in the current precision medicine era, a detailed radiologic-pathologic correlation seems vital to properly evaluate BC.

**Keywords:** Biomarkers, Breast neoplasms, Multiparametric magnetic resonance imaging, Pathology (molecular), Precision medicine

\*Correspondence: veronica.rizzo@uniroma1.it

Department of Radiological, Oncological and Pathological Sciences, Sapienza University of Rome, 00161 Rome, Italy

## Key points

- Early discrimination of the breast cancer subtypes is a key step in treatment planning.
- Molecular subtypes are routinely determined by percutaneous biopsy and immunohistochemical surrogate analysis.
- Multiparametric magnetic resonance imaging could be a valid noninvasive tool for characterising different subtypes of breast cancer.

## Background

Tumour heterogeneity is a well-known characteristic of breast cancer (BC) [1]. With the spread of technologies of molecular biology and the growing knowledge of the biological processes underlying the development of BC, the importance of biomarkers has progressively grown.

Three molecular biomarkers, namely oestrogen receptor, progesterone receptor and human epidermal growth factor receptor 2 (HER2), along with the proliferation index (Ki-67), are currently used, together with traditional parameters (*e.g.*, tumour size, histological grade, and lymph node involvement), in the routine clinical management of BC patients to choose the appropriate treatment and to predict prognosis and tumour response to therapy [1–3]. The molecular subtypes of BC are nowadays routinely determined using immunohistochemical surrogates [4]. According to immunohistochemistry, five subtypes of breast cancer were identified: luminal A-like, luminal B-like HER2 negative, luminal B-like HER2 positive, HER2 positive, and triple negative [5].

Considering the more aggressive clinical behaviour and worse prognosis of triple-negative and HER2 positive BCs as compared to the luminal-like ones, the early discrimination of these molecular subtypes with non-invasive breast imaging may integrate the histopathological results, facilitate the interpretation of histological examination and, ultimately, may be useful to clinicians for planning the most suitable patient management. For this reason, multidisciplinary team meetings (including breast radiologists, pathologists, surgeons, and oncologists) are nowadays considered the best practice in BC management.

Multiparametric magnetic resonance imaging (mpMRI) combines morphologic (T2-weighted sequences), functional (diffusion-weighted imaging, DWI), and kinetic (contrast-enhanced sequences) data, in the attempt to provide information about the development of BC and the response to therapy, among others [6]. Previous studies have suggested that certain BC subtypes show peculiar

features at mpMRI, implying that this technique could differentiate these subtypes noninvasively [7–12].

T2-weighted sequences increase breast MRI specificity, since the great majority of BCs has intermediate to low T2 signal intensity [13, 14], and allow the detection of lesion-associated features, such as intralesional necrosis (commonly accompanying the triple-negative aggressive phenotype) and peritumoural oedema, a suggested indicator of poor prognosis [8, 10]. DWI measures the water diffusivity of the tissues under examination and represents a valuable tool to distinguish benign from malignant breast lesions [15], showing higher specificity than contrast-enhanced sequences [6, 16]. Moreover, DWI has shown the potential to predict lesions aggressiveness, in terms of tumour receptor status [7, 11, 12] and nuclear grading [10, 11, 17]. T1-weighted contrast-enhanced sequences are a key tool in breast mpMRI, having the highest sensitivity and a very good specificity for BC identification. The development of new, abnormal and highly permeable blood vessels (neoangiogenesis) is a fundamental step in cancer growth [18] and represents the basis of BC detection on contrast-enhanced images.

The aim of this study was to verify whether diagnostic breast mpMRI could be used to reliably predict the molecular status of BC in terms of radiologic-pathologic correlation. Accordingly, we investigated the mpMRI features of BC subtypes at 3 T and compared them with immunohistochemical and pathological results.

## Methods

### Study population

This study was conducted according to Good Clinical Practice guidelines and obtained the approval of our institutional review board (no. 0525032019, 25 March 2019). The requirement for informed consent was waived because of the retrospective nature of the study.

From January 2017 to January 2020, patients with a newly diagnosed ultrasound-guided biopsy-proven BC who underwent breast mpMRI at our institution at the time of diagnosis (according to the multidisciplinary team indications) were considered for this study ( $n=364$ ). Ultrasound-guided core needle biopsies were performed by two experienced breast interventional radiologists using a 12 MHz linear probe (SSA-700A; Toshiba, Tokyo, Japan/Affiniti70G; Philips, Amsterdam, Netherlands) and a 14-gauge semiautomatic biopsy needle (Precisa; HS Hospital Service S.p.A., Aprilia, Italy). Definitive breast surgery (including lumpectomy, quadrantectomy and mono- or bilateral mastectomy) was performed within 1 month from mpMRI in all patients.

Exclusion criteria included the following: incomplete MRI examination ( $n=14$ ); previous BC or recurrent disease ( $n=49$ ); ongoing neoadjuvant chemotherapy or other cancer therapy ( $n=45$ ); breast implants ( $n=32$ ); core needle biopsy performed less than 14 days before MRI, to eliminate possible bias due to the diagnostic procedure ( $n=28$ ); and histologic studies or surgery performed in another Institution ( $n=40$ ). Accordingly, 156 patients were included in the study.

Clinical and histopathological data were retrieved from our institutional database (Excel 2011, Microsoft Corporation, Redmond, WA, USA).

### mpMRI technique

All MRI examinations were performed on a 3-T magnet (Discovery MR 750; GE Healthcare, Chicago, IL, USA) using a dedicated 8-channel breast coil compatible with parallel imaging and patients in a prone position. The mpMRI examination protocol used for the study included the following:

- Axial unenhanced two-dimensional fast spin-echo T2-weighted fat-suppressed sequences (repetition time [RT] 9,000–11,000 ms, echo time [ET] 119–120 ms, matrix  $512 \times 224$ , slice thickness 3–5 mm, field of view [FOV]  $350 \times 350$  mm, number of excitations [NEX] 1, scan time 130 s)
- Axial unenhanced two-dimensional DWI echo-planar sequence (RT 4,983–5,314 ms, ET 58 ms, matrix  $150 \times 150$ , slice thickness 3–5 mm, FOV  $350 \times 350$  mm,  $NEX = 2-4$ , scan time 230 s)
- Axial dynamic three-dimensional spoiled gradient-echo T1-weighted fat-suppressed (VIBRANT) sequences (flip angle  $15^\circ$ , RT 8 ms, ET 4 ms, matrix  $512 \times 256$ , slice thickness 1.40 mm, FOV  $380 \times 380$  mm, NEX 1, total scan time 120 s) or axial dynamic dual-echo three-dimensional spoiled gradient-recalled T1-weighted fat-suppressed (DISCO) sequences (flip angle  $15^\circ$ , RT 4 ms, ET 2 ms, bandwidth 166.67 kHz, matrix  $320 \times 320$ , slice thickness 1.40 mm, FOV  $340 \times 340$  mm, NEX 1, total scan time 360 s), VIBRANT sequences were performed before and four times after contrast agent administration and DISCO sequences before and nine times after.
- And sagittal three-dimensional spoiled GE post-contrast T1-weighted sequence (flip angle  $15^\circ$ , RT 4 ms, ET 2 ms, bandwidth 142.86 kHz, matrix  $224 \times 320$ , slice thickness 4 mm, FOV  $300 \times 300$  mm, NEX 1, total scan time 134 s)

Fat suppression of T2-weighted sequences was based on a 3-point Dixon technique (IDEAL), whereas fat suppression of T1-weighted sequences was obtained

using a 2-point Dixon fat–water reconstruction algorithm. DWI echo-planar sequences included  $b$ -values of 0, 500 and  $1,000 \text{ s/mm}^2$ , and the corresponding apparent diffusion coefficient (ADC) maps were calculated automatically. Post-contrast T1-weighted images were acquired after the administration of 0.1 mmol/kg (0.2 mL/kg) of a gadolinium-based contrast agent (Gadoteridol, ProHance; Bracco Imaging Italia S.r.l., Milano, Italy) at a rate of 3 mL/s. Gadoteridol was power injected through a peripheral venous access (22 Gauge) and followed by a 20-mL saline flush at the same rate. Post-processing subtraction images were obtained for the dynamic series of all examinations. Imaging of premenopausal women was performed between the 7th and the 14th day of the menstrual cycle, according to current guidelines [19].

### mpMRI evaluation

MRI datasets were evaluated retrospectively by two experienced breast radiologists (with 18 and 9 years of experience, respectively), in consensus. The readers were blinded to clinical and histopathological information. The evaluation was performed using all the images available, and MRI suspicious findings were classified according to the 2013 American College of Radiology Breast Imaging Reporting and Data System lexicon [20]. All the lesions were measured, and maximum size in mm was reported.

T2-weighted signal intensity of each lesion was evaluated visually and classified as hypointense (lower intensity than the surrounding glandular tissue), isointense (same intensity), and hyperintense (higher intensity), on the basis of the predominant signal intensity of the lesion. Moreover, unenhanced fat-suppressed T2-weighted images were used to evaluate the possible presence of intralesional necrosis and perilesional oedema, assessed visually as areas of high signal intensity (as high as that of water) within or around the lesion.

DWI signal intensity was evaluated qualitatively on high  $b$ -value images ( $b = 1,000 \text{ s/mm}^2$ ). ADC values of DWI hyperintense lesions were obtained drawing manually a two-dimensional region of interest in the centre of the area of restricted diffusion on ADC maps. Considering that a threshold of  $1 \times 10^{-3} \text{ mm}^2/\text{s}$  has been recommended for distinguishing malignant from benign breast lesions, ADC values were classified in very low ( $0.0-0.9 \times 10^{-3} \text{ mm}^2/\text{s}$ ), low ( $1.0-1.3 \times 10^{-3} \text{ mm}^2/\text{s}$ ), and intermediate ( $1.4-1.8 \times 10^{-3} \text{ mm}^2/\text{s}$ ), even if there are no standardised cutoffs yet established [15, 21].

The presence of axillary lymphadenopathies (characterised by size  $> 1$  cm, round shape, loss of the fatty hilum, and cortical thickening) was assessed on post-contrast fat-suppressed T1-weighted sequences.

### Histopathological analysis

All the surgical specimens were sent to the Department of Pathology of our institution and evaluated according to standardised protocols by two experienced pathologists. The samples were fixed in 10% formalin for 12–24 h, processed to obtain paraffin blocks and subsequently cut in 5- $\mu$ m-thick slices and stained with haematoxylin–eosin.

Tumours were classified following the World Health Organization classification [22] and graded according to the Nottingham Histologic Score in low (G1), intermediate (G2), and high grade (G3) of malignancy.

The immunohistochemical analysis was carried out using mouse monoclonal antibodies anti-ER alpha (6F11; Novocastra Laboratories Ltd., Newcastle upon Tyne, UK) and anti-PgR (PgR-312; Novocastra Laboratories Ltd., Newcastle upon Tyne, UK). HER2 evaluation was performed using a semiquantitative immunohistochemical assay (HercepTest; DakoAgilent, Santa Clara, CA, USA). The intensity of HER2 membrane staining was scored as 0, 1+, 2+, or 3+. In case of equivocal result (2+), fluorescence *in situ* hybridisation for HER2 gene amplification was carried out, according to the American Society of Clinical Oncology/College of American Pathologists guidelines [23]. The proliferation index was determined using anti-Ki-67 monoclonal antibody MM1 (Novocastra Laboratories Ltd., Newcastle upon Tyne, UK), and the Ki-67 value was expressed as the percentage of tumour cells showing nuclear staining. According to immunohistochemical features, tumours were classified as luminal A-like, luminal B-like HER2 negative, luminal B-like HER2 positive, HER2 positive and triple-negative, following the St. Gallen Consensus Conference classification [5].

### Statistical analysis

IBM SPSS Statistics v.25 (Chicago, IL, USA) was used to perform statistical analyses,  $p$ -values < 0.05 being considered significant. The Kolmogorov–Smirnov  $Z$ -test was

performed to assess the normality of the distribution for the continuous variables tested. Continuous normal variables were expressed as mean  $\pm$  standard deviation, while continuous nonnormal variables were expressed as median and range. Categorical variables were compared using the  $\chi^2$  test. The Bonferroni correction was used for post hoc  $\chi^2$  analysis. Univariate and multivariate logistic regression analyses were performed to identify the predicting value of imaging-derived features associated with the different molecular subtypes of BC. All variables with a  $p$ -value < 0.05 at univariate analysis were included in the multivariate analysis.

## Results

### Study population

A total of 156 patients were included in this study, 15 were affected by ductal carcinoma *in situ* (DCIS), 122 by invasive carcinoma of no special type (NST) and 19 by invasive lobular carcinoma (ILC). The 141 invasive BCs detected at histological evaluation were categorised according to the St. Gallen classification as luminal A-like ( $n=45$ ), luminal B-like (HER2 positive and HER2 negative) ( $n=54$ ), HER2 positive ( $n=5$ ) and triple negative ( $n=37$ ). Patients' mean age was 53.8 (standard deviation 10.7). Median size of BCs at MRI was 20 mm (range 6–100 mm).

### Invasive carcinomas and DCIS

On MRI examination, the vast majority of invasive lesions appeared as mass enhancements (80.8%), while DCISs appeared as non-mass enhancements (86.7%) (Fig. 1). Statistical analysis demonstrated a significant association between invasive NST carcinoma and mass enhancement, intralesional necrosis, axillary adenopathy and multifocal extension of disease. We also observed a significant association between DCIS and isointensity on T2-weighted images, non-mass enhancement and the absence of central necrosis and of axillary adenopathy.

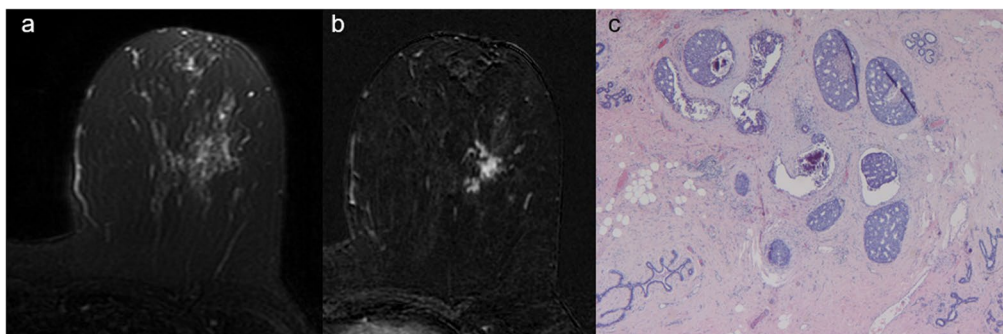


**Fig. 1** A 59-year-old woman with ductal carcinoma *in situ* of the left breast. **a** Axial fat-suppressed T2-weighted image shows a 21-mm isointense lesion in the lower outer quadrant of the left breast. **b** Axial post-contrast T1-weighted subtracted images show a corresponding regional, clumped non-mass enhancement. **c** Histological examination confirms the suspicion of *in situ* carcinoma highlighting several intraductal calcifications

No association was found between ILC and MRI features. Further details are shown in Table 1.

### Grading

A total of 63 lesions were characterised by a low or intermediate grade of differentiation (G1 or G2) and 73 by a high grade of differentiation (G3). The remaining 20 lesions were not classifiable at histopathological analysis. Statistical analyses found a significant association between G3 tumours and rim enhancement, intralesional necrosis, peritumoural oedema, axillary adenopathy, and multifocal disease. The univariate analysis proved that rim enhancement, intralesional necrosis, peritumoural oedema, the presence of malignant axillary lymph nodes, and very low ADC values were predictors of high grade of malignancy. The multivariate analysis confirmed rim enhancement as the only independent predictor for high grade of malignancy (Table 2).

### Tumour size

Median invasive BCs size at MR imaging was 53 mm (range 6–100 mm); 44% of the lesions were <2 cm in size, while 56% were  $\geq 2$  cm. There was a significant association between lesion size <2 cm and luminal A-like tumours. No statistical association was found between tumour size and the other molecular subtypes, even if luminal B and triple negatives resulted to be larger than the others (Fig. 2).

### Luminal A-like tumours

Most luminal A-like tumours were mass lesions (77.8%) characterised by irregular shape (42.9%), non-circumscribed margins (94.3%) and the absence of rim enhancement (91.4%) (Fig. 3). Statistical analyses showed a significant association between luminal A-like status and the absence of rim enhancement, of intralesional necrosis, of peritumoural oedema and of axillary adenopathy. The univariate regression analysis showed that lesion size  $\geq 2$  cm, rim enhancement, intralesional necrosis, peritumoural oedema and axillary pathological lymph nodes were negative predictors of luminal A-like cancers. The multivariate analysis confirmed that the absence of rim enhancement was independently associated with luminal A-like lesions (Table 3).

### Luminal B-like tumours

Most luminal B-like were mass lesions (81.5%), characterised by round shape (56.8%), non-circumscribed margins (77.3%) and the absence of rim enhancement (63.7%).  $\chi^2$  analyses showed an inverse association between luminal B-like tumours and multicentric disease. Regression analyses proved that multicentric disease is a negative predictor of luminal B status (Table 4).

### HER2-positive tumours

All the 5 HER2-positive tumours included in our study population were masses characterised by

**Table 1** Association between histological subtypes of breast cancer

		DCIS	$\chi^2$ analysis p-value	Invasive carcinoma no special type	$\chi^2$ analysis p- value	ILC	$\chi^2$ analysis p-value
No. of patients		15		122		19	
Tumour size	Median (mm)	38		20		26	
	Range (mm)	7–72		6–90		8–100	
$\geq 2$ cm		10/15	0.429	65/122	0.071	14/19	0.118
T2 intensity	Hypointensity	0/15	<0.001	55/122	0.015 <sup>a</sup>	9/19	0.833
	Isointensity	12/15		30/122		5/19	
	Hyperintensity	3/15		37/122		5/19	
Mass enhancement		2/15	<0.001	102/122	<0.001	12/19	0.233
Rim enhancement		0/2	0.292	39/102	0.079	2/12	0.153
Intralesional necrosis		0/15	0.001	53/122	0.035	8/19	0.775
Perilesional oedema		6/15	0.358	67/122	0.085	7/19	0.179
Axillary adenopathy		0/15	0.003	48/122	0.007	5/19	0.452
Intensity-to-time curve	Type I	1/15	0.801	10/122	0.877	2/19	0.932
	Type II	5/15		31/122		5/19	
	Type III	9/15		81/122		12/19	
ADC value	Very low	3/10	0.055	70/111	0.144	7/14	0.575
	Low	6/10		39/111		7/14	
	Intermediate	1/10		2/111		0/14	
Extent of disease	Unifocal	7/15	0.018 <sup>a</sup>	55/122	0.02	9/19	0.170
	Multifocal	0/15		39/122		2/19	
	Multicentric	8/15		28/122		8/19	

<sup>a</sup> Bonferroni's post hoc analysis found no significance. ADC Apparent diffusion coefficient, DCIS Ductal carcinoma in situ, ILC Invasive lobular carcinoma

**Table 2** Association between breast cancer grading (high grade) and magnetic resonance imaging features

		High grade	$\chi^2$ analysis p-value	Univariate analysis OR (CI 95%) <sup>b</sup>	p-value	Multivariate analysis OR (CI 95%) <sup>b</sup>	p-value
<b>No. of patients</b>		73					
<b>Tumour size</b>	Median (mm)	52					
	Range (mm)	34–75					
<b>≥ 2 cm</b>		44/73	0.097	1.779 (0.899–3.518)	0.098		
<b>T2 intensity</b>	Hypointensity	35/73	0.047 <sup>a</sup>	1.842 (0.918–3.697)	0.086	0.385 (0.124–1.193)	0.098
	Isointensity	16/73		0.399 (0.189–0.844)	0.016		
	Hyperintensity	22/73		1.267 (0.595–2.699)	0.539		
<b>Mass enhancement</b>		55/73	0.921	1.040 (0.478–2.264)	0.921		
<b>Rim enhancement</b>		25/55	0.002	4.062 (1.607–10.271)	0.003	3.689 (1.011–3.467)	0.048
<b>Intralesional necrosis</b>		33/73	0.028	2.232 (1.084–4.597)	0.029	0.651 (0.193–2.195)	0.489
<b>Perilesional oedema</b>		45/73	0.001	3.214 (1.588–6.505)	0.001	2.105 (0.729–6.078)	0.169
<b>Axillary adenopathy</b>		32/73	0.008	2.732 (1.287–5.799)	0.009	2.241 (0.769–6.536)	0.139
<b>Intensity-to-time curve</b>	Type I	2/73	0.245	0.268 (0.052–1.377)	0.115		
	Type II	21/73		1.093 (0.515–2.319)	0.817		
	Type III	50/73		1.250 (0.613–2.548)	0.539		
<b>ADC value</b>	Very low	41/60	0.036 <sup>a</sup>	2.937 (1.385–6.228)	0.005	2.191 (0.806–5.951)	0.124
	Low	18/60		0.339 (0.159–0.723)	0.005		
	Intermediate	1/60		0.873 (0.053–14.29)	0.924		
<b>Extent of disease</b>	Unifocal	29/73	0.011	0.494 (0.249–0.980)	0.044	2.247 (0.771–6.548)	0.138
	Multifocal	27/73		3.522 (1.504–8.246)	0.004		
	Multicentric	17/73		0.759 (0.351–1.640)	0.483		

<sup>a</sup> Bonferroni’s post hoc analysis found no significance. <sup>b</sup>OR Odds ratio, CI Confidence interval, ADC Apparent diffusion coefficient

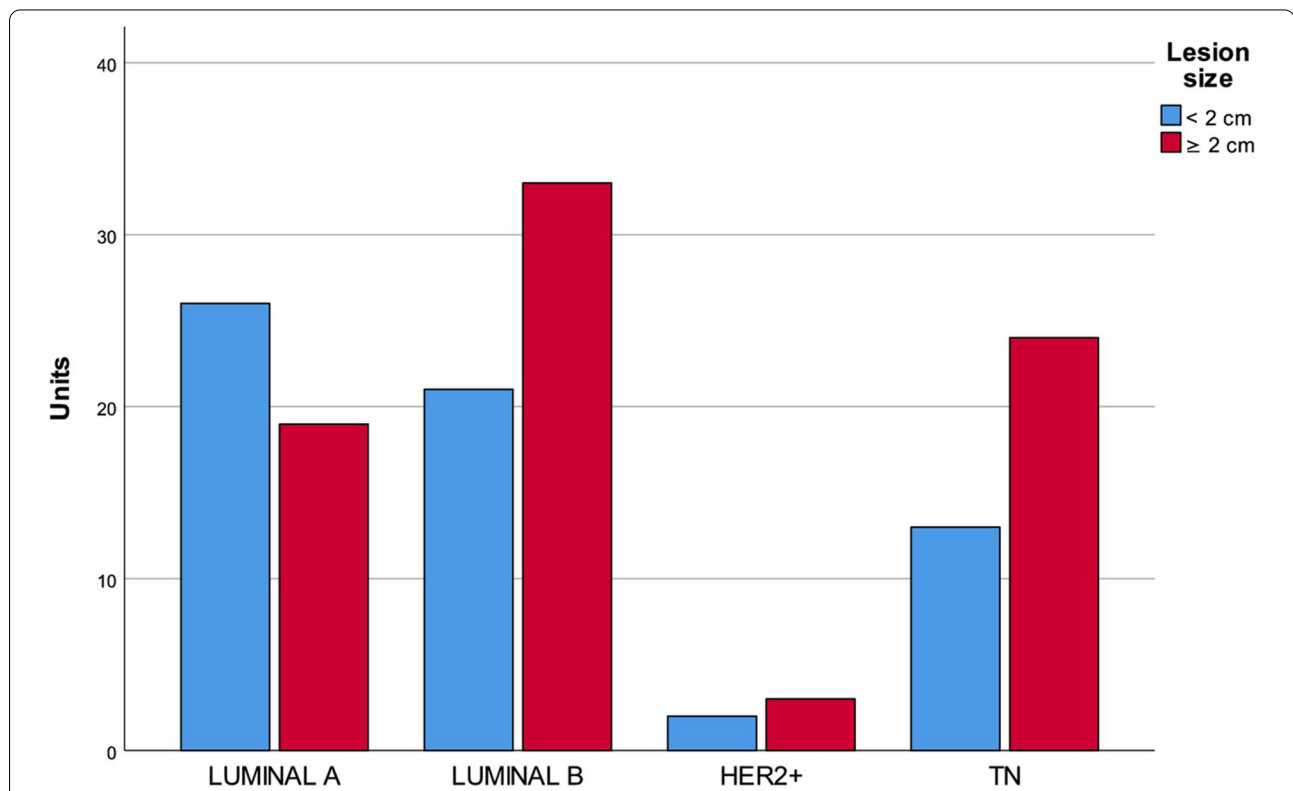


**Fig. 2** Distribution of the molecular subtypes of breast cancer (luminal A-like, luminal B-like, HER2 positive, and triple negative) according to lesions size

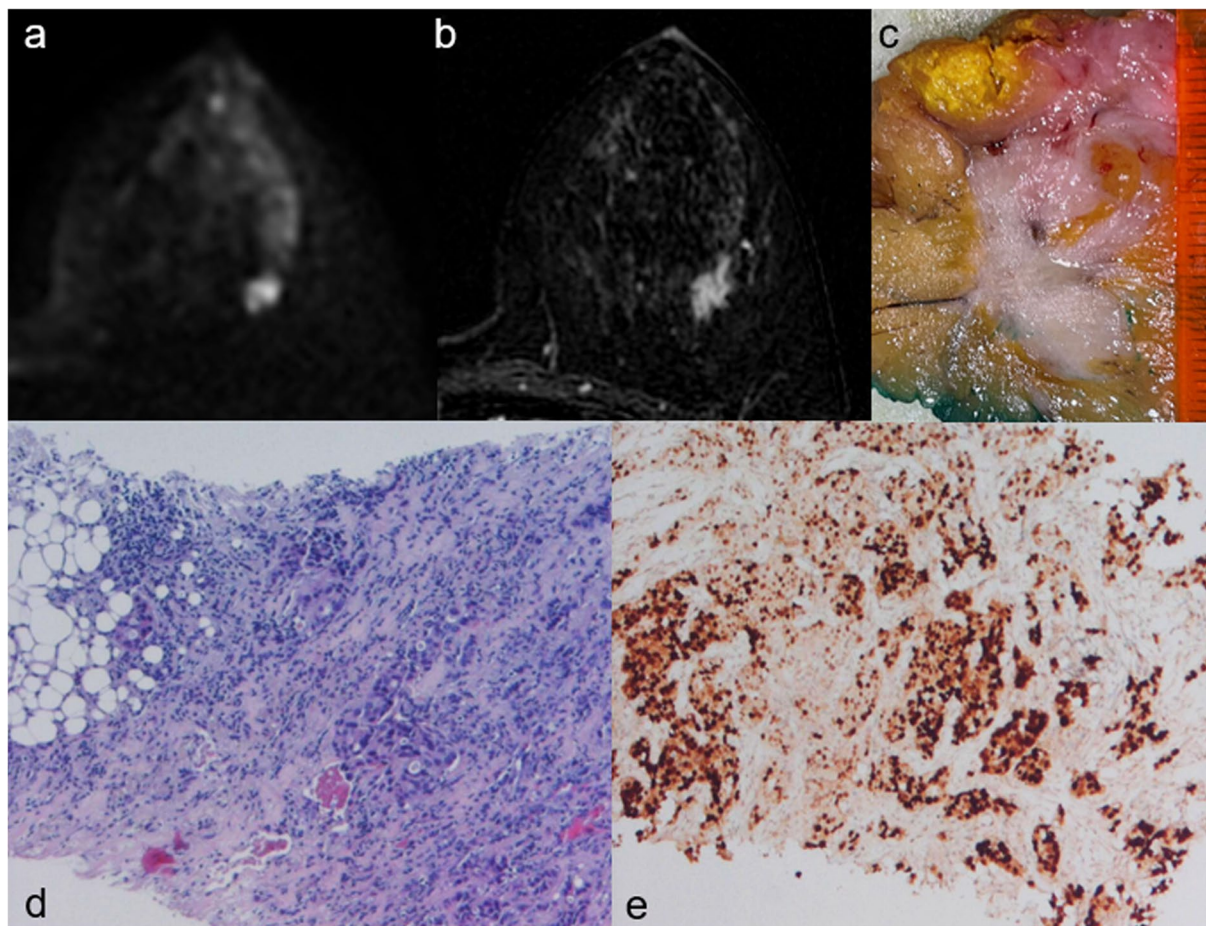


**Fig. 3** A 42-year-old woman with a luminal A-like carcinoma in the outer upper quadrant of the left breast. **a** Axial diffusion-weighted image ( $b$ -value = 1,000 s/mm.<sup>2</sup>) shows the high signal intensity of the mass, corresponding to a restricted diffusion area. **b** Axial post-contrast T1-weighted subtracted image shows a 14-mm mass with irregular shape, spiculated margins, and heterogeneous enhancement. **c** On cut surface, the lesion has irregular and infiltrative borders. **d–e** Histologic examination confirms the diagnosis of infiltrating carcinoma of “no special type” with diffuse expression of oestrogen receptor on immunohistochemistry

non-circumscribed margins, heterogeneous enhancement and without peritumoural oedema. Only one of them (20.0%) showed intralesional necrosis.  $\chi^2$  analysis showed an inverse association between HER2-positive cancers and peritumoural oedema, although regression analyses showed no significant predictors (Table 5).

#### **Triple negative tumours**

Most triple negative tumours were masses (81.1%) characterised by round shape (86.7%), non-circumscribed margins (90%) and rim enhancement (73.3%) (Fig. 4). Statistical analyses showed a significant association between triple-negative tumours and round shape, rim enhancement, intralesional necrosis and the presence of peritumoural oedema (Table 6). The univariate regression analysis proved that round shape in mass lesions, rim

enhancement, intralesional necrosis and peritumoural oedema were predictors of triple negative lesions, while low ADC value was a negative predictor. The multivariate analysis confirmed that round shape in mass lesions, rim enhancement, and peritumoural oedema were associated with triple negatives (Table 6).

#### **Discussion**

BC is a heterogeneous disease, with distinct molecular subtypes which have both prognostic and predictive value. In this context, precision medicine involves the use of biomarkers to create customised treatments. Furthermore, the possibility to draw a reliable correlation between molecular subtypes and imaging features of BC is envisaged to improve patients' care. As a consequence, nowadays, imaging aims to offer a complementary, non-invasive method to obtain biological information about

**Table 3** Association between luminal A-like breast cancer and magnetic resonance imaging features

	Luminal A	$\chi^2$ p-value	Univariate analysis		Multivariate analysis	
			OR (CI 95%) <sup>a</sup>	p-value	OR (CI 95%) <sup>a</sup>	p-value
<b>No. of patients</b>	45					
<b>Tumour size</b>	Median (mm) Range (mm)	18 6–100				
<b>≥ 2 cm</b>		19/45	0.024	0.438 (0.213–0.902)	0.025	0.411 (0.151–1.118)
<b>T2 intensity</b>	Hypointensity Isointensity Hyperintensity	20/45 12/45 13/45	0.941	0.945 (0.464–1.927) 1.154 (0.513–2.595) 0.939 (0.431–2.043)	0.877 0.729 0.873	
<b>Mass enhancement</b>		35/45	0.525	0.753 (0.313–1.810)	0.526	
<b>Rim enhancement</b>		3/35	<0.001	0.101 (0.029–0.358)	<0.001	0.163 (0.040–0.657)
<b>Intralesional necrosis</b>		10/45	0.001	0.252 (0.112–0.566)	0.001	0.711 (0.228–2.220)
<b>Perilesional oedema</b>		12/45	<0.001	0.199 (0.091–0.436)	<0.001	0.419 (0.149–1.175)
<b>Abnormal lymph nodes</b>		10/45	0.01	0.352 (0.157–0.791)	0.012	0.600 (0.212–1.693)
<b>Intensity-to-time curve</b>	Type I Type II Type III	4/45 11/45 30/45	0.977	1.073 (0.306–3.769) 0.919 (0.405–2.083) 1.048 (0.495–2.216)	0.912 0.839 0.903	
<b>ADC value</b>	Very low Low Intermediate	20/40 19/40 1/40	0.182	0.491 (0.228–1.058) 1.944 (0.899–4.200) 2.154 (0.131–35.34)	0.069 0.091 0.591	
<b>Extent of disease</b>	Unifocal Multifocal Multicentric	19/45 10/45 16/45	0.148	0.828 (0.405–1.692) 0.599 (0.263–1.364) 2.097 (0.957–4.593)	0.605 0.222 0.064	

<sup>a</sup> OR Odds ratio, CI Confidence interval, ADC Apparent diffusion coefficient

**Table 4** Correlation between luminal B-like tumours and MRI features

	Luminal B	$\chi^2$ analysis p-value	Univariate analysis	
			OR (CI 95%) <sup>a</sup>	p-value
<b>No. of patients</b>	54			
<b>Tumour size</b>	Median (mm) Range (mm)	20 6–86		
<b>≥ 2 cm</b>		33/54	0.338	1.401 (0.702–2.793)
<b>T2 intensity</b>	Hypointensity Isointensity Hyperintensity	29/54 9/54 16/54	0.159	1.723 (0.868–3.420) 0.469 (0.201–1.098) 0.988 (0.470–2.076)
<b>Mass enhancement</b>		44/54	0.881	1.069 (0.449–2.544)
<b>Rim enhancement</b>		16/44	0.944	1.029 (0.469–2.255)
<b>Intralesional necrosis</b>		23/54	0.899	0.957 (0.482–1.900)
<b>Perilesional oedema</b>		32/54	0.204	1.558 (0.784–3.097)
<b>Abnormal lymph nodes</b>		23/54	0.334	1.410 (0.702–2.831)
<b>Intensity-to-time curve</b>	Type I Type II Type III	5/54 14/54 35/54	0.961	1.166 (0.351–3.877) 1.034 (0.475–2.250) 0.921 (0.451–1.882)
<b>ADC value</b>	Very low Low Intermediate	29/48 19/48 0/48	0.490	0.922 (0.440–1.932) 1.213 (0.576–2.554) Out of scale
<b>Extent of disease</b>	Unifocal Multifocal Multicentric	28/54 19/54 7/54	0.025	1.526 (0.770–3.022) 1.604 (0.766–3.357) 0.298 (0.120–0.740)

<sup>a</sup> OR Odds ratio, CI Confidence interval, ADC Apparent diffusion coefficient



**Table 5** Correlation between HER2-positive tumours and magnetic resonance imaging features

		HER2+	$\chi^2$ analysis <i>p</i> -value	Univariate analysis OR (CI 95%) <sup>a</sup>	<i>p</i> -value
<b>No. of patients</b>		5			
<b>Tumour size</b>	Median (mm)	25			
	Range (mm)	12–36			
<b>≥ 2 cm</b>		3/5	0.885	1.184 (0.192–7.316)	0.856
<b>T2 intensity</b>	Hypointensity	3/5	0.322	1.844 (0.299–11.39)	0.510
	Isointensity	2/5		2.081 (0.333–12.99)	0.433
	Hyperintensity	0/5		Out of scale	
<b>Mass enhancement</b>		5/5	0.268	Out of scale	
<b>Rim enhancement</b>		0/5	0.087	Out of scale	
<b>Intralesional necrosis</b>		1/5	0.285	0.317 (0.034–2.908)	0.309
<b>Perilesional oedema</b>		0/5	0.017	Out of scale	
<b>Abnormal lymph nodes</b>		2/5	0.910	1.111 (0.180–6.875)	0.910
<b>Intensity-to-time curve</b>	Type I	0/5	0.720	Out of scale	0.774
	Type II	1/5		0.721 (0.078–6.674)	0.509
	Type III	4/5		2.112 (0.230–19.442)	
<b>ADC value</b>	Very low	4/5	0.681	2.575 (0.279–23.75) 0.417 (0.045–3.845)	0.404
	Low	1/5		Out of scale	0.440
	Intermediate	0/5			
<b>Extent of disease</b>	Unifocal	2/5	0.857	0.796 (0.129–4.915) 1.658 (0.267–10.31)	0.806
	Multifocal	2/5		0.721 (0.078–6.674)	0.588
	Multicentric	1/5			0.774

<sup>a</sup> OR Odds ratio, CI Confidence interval, ADC Apparent diffusion coefficient

BC, in addition to traditional tissue-sampling-derived biomarkers.

Breast MRI is considered the more promising technique to differentiate tumour subtypes noninvasively [6, 16]. Contrast-enhanced sequences are the backbone of any breast MRI protocol, providing information about morphological and kinetic features of BC. To overcome the

suboptimal specificity of contrast-enhanced MRI, functional techniques, such as MR spectroscopy and DWI, have been widely investigated and progressively introduced into routine clinical practice. Nowadays, a basic mpMRI protocol includes unenhanced sequences (T2 weighted and DWI) followed by the series of pre- and post-contrast T1-weighted acquisitions [13], since it was demonstrated

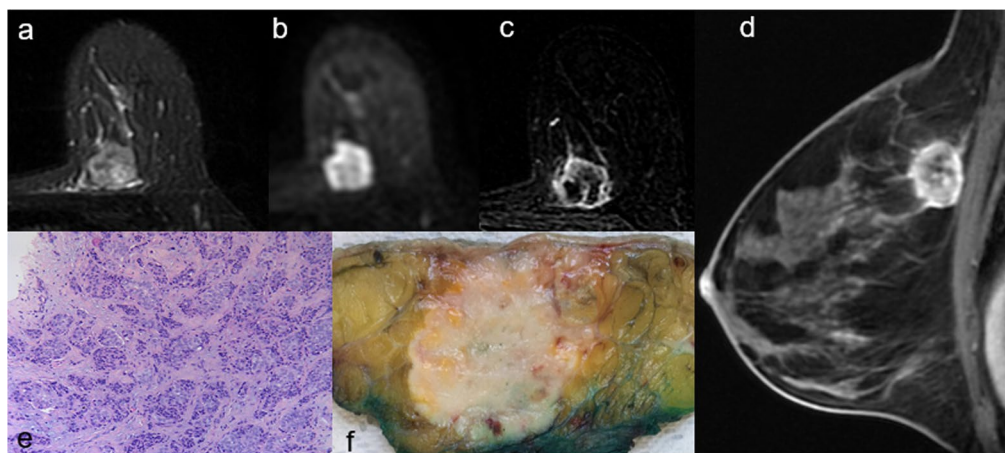


**Fig. 4** A 45-year-old woman with triple-negative tumour of the left breast. **a** Axial fat-suppressed T2-weighted image shows an 18-mm, heterogeneously hyperintense round mass with non-circumscribed margins in the upper inner quadrant of the left breast. **b** Axial diffusion-weighted imaging ( $b$ -value = 1,000 s/mm<sup>2</sup>) shows peripheral high signal intensity and central hypointensity. **c** Axial and **(d)** sagittal post-contrast T1-weighted subtracted images show a corresponding irregular round mass with rim enhancement. **e** On cut surface, the lesion is round shaped with smooth margins. **f** Histologic examination confirms the diagnosis of infiltrating carcinoma of “no special type”

**Table 6** Correlation between triple-negative tumours and magnetic resonance imaging features

	Triple negative	$\chi^2$ analysis p-value	Univariate analysis		Multivariate analysis	
			OR (CI 95%) <sup>a</sup>	p-value	OR (CI 95%) <sup>a</sup>	p-value
<b>No. of patients</b>	37					
<b>Tumour size</b>	Median (mm) Range (mm)	23 9–90				
<b>≥ 2 cm</b>		24/37	0.207	1.645 (0.756–3.577)	0.209	
<b>T2 intensity</b>	Hypointensity Isointensity Hyperintensity	12/37 12/37 13/37	0.173	0.480 (0.218–1.056) 1.690 (0.737–3.875) 1.401 (0.630–3.116)	0.068 0.215 0.409	
<b>Mass enhancement</b>		30/37	0.967	1.020 (0.392–2.655)	0.967	
<b>Shape (Mass)</b>	Round Oval Irregular	26/30 0/30 4/30	0.001	7.150 (2.295–22.28) Out of scale 0.205 (0.066–0.640)	0.001 0.006	5.319 (1.425–19.85)
<b>Rim enhancement</b>		22/30	<0.001	9.408 (3.613–24.50)	<0.001	9.155 (2.537–33.04)
<b>Intralesional necrosis</b>		27/37	<0.001	5.559 (2.416–12.79)	<0.001	0.846 (0.214–3.340)
<b>Perilesional oedema</b>		30/37	<0.001	5.844 (2.352–14.52)	<0.001	3.852 (1.092–13.59)
<b>Abnormal lymph nodes</b>		18/37	0.106	1.868 (0.871–4.003)	0.108	
<b>Intensity-to-time curve</b>	Type I Type II Type III	3/37 10/37 24/37	0.969	0.931 (0.238–3.644) 1.111 (0.475–2.601) 0.936 (0.426–2.059)	0.919 0.808 0.870	
<b>ADC value</b>	Very low Low Intermediate	24/32 7/32 1/32	0.106	2.264 (0.921–5.565) 0.388 (0.152–0.986) 2.968 (0.180–48.88)	0.075 0.047 0.447	4.762 (0.018–1277)
<b>Extent of disease</b>	Unifocal Multifocal Multicentric	15/37 10/37 12/37	0.530	0.765 (0.358–1.638) 0.872 (0.377–2.017) 1.600 (0.701–3.654)	0.491 0.749 0.265	

<sup>a</sup> OR Odds ratio, CI Confidence interval, ADC Apparent diffusion coefficient

that mpMRI including contrast-enhanced sequences and DWI increases diagnostic accuracy in BC diagnosis [16, 24]. Also, magnetic resonance spectroscopy improves the diagnostic accuracy of breast MRI [25–29]; however, technical challenges and operator dependency have limited large-scale implementation of this technique [30].

The purpose of our study was to clarify whether diagnostic mpMRI at 3 T could be a reliable noninvasive predictor of histological tumour type and molecular subtype of BC. Most of the patients included in this study (78.2%) were affected by invasive carcinoma NST, which is the most common type of BC, 12% by ILC, and about 10% by DCIS. Our distribution substantially reflected data reported in literature [31–35].

The specific features of DCIS are calcifications at digital mammography (70–90% of cases [36]) and non-mass enhancement at MRI contrast-enhanced sequences (up to 81% of cases [34, 37–39]); our results (86.7% of DCIS presented as non-mass enhancements,  $p < 0.001$ ) are in substantial agreement with those data. A second MRI feature significantly associated with DCIS was T2

isointensity (78.6%,  $p < 0.001$ ) (Fig. 1), also in agreement with data reported in literature too [39]. DCIS was significantly associated with the absence of axillary adenopathy (0%,  $p = 0.003$ ); this result was expected, since DCIS is confined to the mammary ductal lobular system, without invasion of the basement membrane. However, the occurrence of lymph node metastases is still possible (likely due to missing areas of microinvasion in large-sized tumours or iatrogenic dissemination of tumour cells during preoperative breast biopsy [36]).

The term invasive carcinoma NST identifies a subset of invasive BCs that cannot be classified morphologically as any of the special histological types. ILC, instead, is characterised by a typical discohesive morphology and by the loss of E-cadherin function. The small cohort of ILC included in the study (although reflecting data in literature [31–33]) could explain the lack of statistical significance of our results. On the contrary, MRI features significantly associated with invasive carcinomas NST were as follows: mass enhancement, intralesional necrosis and abnormal axillary lymph nodes. The majority of

invasive BCs appear as masses with intermediate to low signal intensity on T2-weighted images, due to high cellularity and low water content [13]; our results are in line with these findings. The contemporary association between invasive BC of NST and intralesional necrosis (that shows high signal on T2-weighted images by definition [7]) can be explained by the fact that the evaluation of T2-signal intensity in this study was based on the predominant signal intensity of each lesion; therefore, lesions with only small areas of intralesional necrosis were still classified as isointense or hypointense.

As expected, rim enhancement, intralesional necrosis, peritumoural oedema and the presence of metastatic axillary lymph nodes were predictors of G3 status. These results emphasise the evidence that poorly differentiated, aggressive BCs are associated with poor prognostic indicators at breast MRI. Moreover, we showed an inverse correlation between tumour grading and ADC values, since very low ADC values were significantly associated with high tumour grades. This result has confirmed the predicting value of DWI regarding nuclear grading, as suggested by a few previous studies [10, 11, 17].

The vast majority of invasive breast lesions included in this study were luminal-like (70.2%), while triple-negative and HER2-positive cases represented a minority of the sample (26.2% and 3.6%, respectively). These data reflect the lower frequency of these molecular subtypes and are comparable to similar series in literature [40, 41]. In this study, luminal-like and HER2-positive BCs were more frequently characterised by irregular shape. In particular, most luminal A-like were irregular-shaped (42.9%) masses (77.8%), with non-circumscribed margins (94.3%) and without rim enhancement (91.4%).

Furthermore, our study has demonstrated that the absence of MRI features on T2-weighted images associated with poor prognosis, such as intralesional necrosis [42] and peritumoural oedema [43, 44], was significantly associated with luminal A-like tumours (Fig. 3). In particular, the absence of peritumoural oedema resulted independently associated with the luminal A-like status, in agreement with previous studies [8, 10, 45]. Finally, luminal A-like tumours in our study were significantly associated with the absence of axillary adenopathy, confirming that this BC subtype is characterised by a less aggressive behaviour and a better prognosis [46].

Triple negative BCs are biologically and clinically aggressive tumours with peculiar imaging features, on both conventional breast imaging (frequently mimicking benign lesions [47–49]) and MRI. In our study, triple negative BCs were predominantly masses (81.1%), characterised by round shape (86.7%), non-circumscribed margins

(90%) and rim enhancement (73.3%). Round shape and rim enhancement were independently associated with the triple-negative status (Fig. 4). These data confirm existing evidence in literature [7, 9, 10, 45, 50–54]. The typical regular shape can be explained by the frequent occurrence of “pushing”, non-infiltrative growth pattern of triple negatives compared to other subtypes of BC, while the presence of rim enhancement on contrast-enhanced sequences has been associated with increased angiogenesis and vascular endothelial growth factor expression and with the lack of oestrogen and progesterone receptors [55, 56]. Among MRI features on T2-weighted images, intralesional necrosis and peritumoural oedema have proved to be positive predictor of the triple-negative status. These results are in accordance with previous literature [7, 8, 10, 45, 50, 53].

Our study has some limitations. First, it was a single-centre, retrospective study, and the cohort of patients enrolled was relatively small, and the number of triple-negative and HER2-positive BCs was even smaller, because those patients tend to receive neoadjuvant chemotherapy. Secondly, MRI datasets were evaluated by two readers, in consensus, not considering interobserver variability. In addition, due to technical problems, percutaneous biopsies under mammographic guidance were not performed during the enrolment period, and this could have caused an underestimation of the number of DCIS cases. Finally, molecular subtypes were determined using immunohistochemical surrogates, which lack in standardisation compared to gene profiling, even if they have shown similar clinical significance and are nowadays routinely used [4].

In conclusion, we showed that mpMRI at 3-T MRI has proved to be a valid noninvasive tool to distinguish between BC subtypes, especially luminal A-like and triple negative, even though histopathology remains the standard of care also in the present time of rapid development of advanced breast imaging.

#### Abbreviations

ADC: Apparent diffusion coefficient; BC: Breast cancer; DCIS: Ductal carcinoma *in situ*; DWI: Diffusion-weighted imaging; ET: Echo-time; FOV: Field of view; HER2: Human epidermal growth factor receptor 2; ILC: Invasive lobular carcinoma; Ki-67: Proliferation index; mpMRI: Multiparametric magnetic resonance imaging; NEX: Number of excitations; NST: No special type; RT: Repetition time.

#### Authors' contributions

Conceptualisation, FG and FP; methodology, FG, VR, GM, and BC; validation, FP and GdA; formal analysis, FG, VR, and GM; investigation, VR, CC, EK, and BC; data curation, VR, CC, and EK; writing—original draft preparation, VR and GM; writing—review and editing, FG; and supervision, FP and GdA. The author(s) read and approved the final manuscript.

#### Funding

This research received no external funding.

**Availability of data and materials**

The datasets generated during and/or analysed during the current study are available from the corresponding author on reasonable request.

**Declarations****Ethics approval and consent to participate**

This study was conducted according to Good Clinical Practice guidelines and obtained the approval of our institutional review board (no. 0525032019, 25 March 2019). The requirement for informed consent was waived because of the retrospective nature of the study.

**Consent for publication**

Not applicable.

**Competing interests**

The authors declare that they have no competing interests.

Received: 23 December 2021 Accepted: 3 June 2022

Published online: 08 August 2022

**References**

- Harbeck N, Gnant M (2017) Breast cancer. *Lancet* 18:1134–1150. [https://doi.org/10.1016/S0140-6736\(16\)31891-8](https://doi.org/10.1016/S0140-6736(16)31891-8)
- Coates AS, Winer EP, Goldhirsch A et al (2015) Tailoring therapies—improving the management of early breast cancer: St Gallen International Expert Consensus on the Primary Therapy Of Early Breast Cancer 2015. *Ann Oncol* 26:1533–1546. <https://doi.org/10.1093/annonc/mdv221>
- Vuong D, Simpson PT, Green B, Cummings MC, Lakhani SR (2014) Molecular classification of breast cancer. *Virchows Arch* 465:1–14. <https://doi.org/10.1007/s00428-014-1593-7>
- Tang P, Tse GM (2016) Immunohistochemical surrogates for molecular classification of breast carcinoma: a 2015 update. *Arch Pathol Lab Med* 140:806–814. <https://doi.org/10.5858/arpa.2015-0133-RA>
- Goldhirsch A, Wine EP, Coates AS et al (2013) Panel Members. Personalizing the treatment of women with early breast cancer: highlights of the St Gallen International Expert Consensus on the Primary Therapy of Early Breast Cancer. *Ann Oncol* 24:2206–2223. <https://doi.org/10.1093/annonc/mdt303>
- Marino MA, Helbich T, Baltzer P, Pinker-Domenig K (2018) Multiparametric MRI of the breast: a review. *J Magn Reson Imaging* 47:301–315. <https://doi.org/10.1002/jmri.25790>
- Moffa G, Galati F, Collalunga E et al (2020) Can MRI biomarkers predict triple-negative breast cancer? *Diagnostics (Basel)* 10:1090. <https://doi.org/10.3390/diagnostics10121090>
- Panzironi G, Moffa G, Galati F, Marzocca F, Rizzo V, Pediconi F (2020) Peritumoral edema as a biomarker of the aggressiveness of breast cancer: results of a retrospective study on a 3 T scanner. *Breast Cancer Res Treat* 181:53–60. <https://doi.org/10.1007/s10549-020-05592-8>
- Vilar LN, Alandete Germán SP, Medina García R, Blanc García E, Camarasa Lillo N, Vilar Samper J (2017) MR imaging findings in molecular subtypes of breast cancer according to BIRADS system. *Breast J* 23:421–428. <https://doi.org/10.1111/tbj.12756>
- Costantini M, Belli P, Distefano D et al (2012) Magnetic resonance imaging features in triple-negative breast cancer: comparison with luminal and HER2-overexpressing tumors. *Clin Breast Cancer* 12:331–339. <https://doi.org/10.1016/j.clbc.2012.07.002>
- Martincich L, Deantoni V, Bertotto I et al (2012) Correlations between diffusion-weighted imaging and breast cancer biomarkers. *Eur Radiol* 22:1519–1528. <https://doi.org/10.1007/s00330-012-2403-8>
- Youk JH, Son EJ, Chung J, Kim JA, Kim EK (2012) Triple-negative invasive breast cancer on dynamic contrast-enhanced and diffusion-weighted MR imaging: comparison with other breast cancer subtypes. *Eur Radiol* 22:1724–1734. <https://doi.org/10.1007/s00330-012-2425-2>
- Mann RM, Cho N, Moy L (2019) Breast MRI: state of the art. *Radiology* 292:520–536. <https://doi.org/10.1148/radiol.2019182947>
- Arponen O, Masarwah A, Sutela A et al (2016) Incidentally detected enhancing lesions found in breast MRI: analysis of apparent diffusion coefficient and T2 signal intensity significantly improves specificity. *Eur Radiol* 26:4361–4370. <https://doi.org/10.1007/s00330-016-4326-2>
- Baltzer P, Mann RM, Lima M et al (2020) EUSOBI International Breast Diffusion-Weighted Imaging working group. Diffusion-weighted imaging of the breast—a consensus and mission statement from the EUSOBI International Breast Diffusion-Weighted Imaging working group. *Eur Radiol* 30:1436–1450. <https://doi.org/10.1007/s00330-019-06510-3>
- Pinker K, Helbich TH, Morris EA (2017) The potential of multiparametric MRI of the breast. *Br J Radiol* 90:20160715. <https://doi.org/10.1259/bjr.20160715>
- Rizzo V, Moffa G, Kripa E, Caramanico C, Pediconi F, Galati F (2021) Pre-operative staging in breast cancer: intraindividual comparison of unenhanced MRI combined with digital breast tomosynthesis and dynamic contrast enhanced-MRI. *Front Oncol* 11:661945. <https://doi.org/10.3389/fonc.2021.661945>
- Hanahan D, Weinberg RA (2000) The hallmarks of cancer. *Cell* 100:57–70. [https://doi.org/10.1016/S0092-8674\(00\)81683-9](https://doi.org/10.1016/S0092-8674(00)81683-9)
- Mann RM, Balleyguier C, Baltzer PA et al (2015) European Society of Breast Imaging (EUSOBI), with language review by Europa Donna - the European Breast Cancer Coalition. Breast MRI: EUSOBI recommendations for women's information. *Eur Radiol* 25:3669–3678. <https://doi.org/10.1007/s00330-015-3807-z>
- Morris EA, Comstock CE, Lee CH et al (2013) ACR BI-RADS magnetic resonance imaging. In ACR BI-RADS Atlas, Breast Imaging Reporting and Data System, 5th edn. American College of Radiology, Reston
- Surov A, Meyer HJ, Wienke A (2019) Can apparent diffusion coefficient (ADC) distinguish breast cancer from benign breast findings? A meta-analysis based on 13 847 lesions. *BMC Cancer* 19:955. <https://doi.org/10.1186/s12885-019-6201-4>
- WHO Classification of Tumours Editorial Board (2019) In WHO Classification of Tumours, 5th edn. IARC Publications, Lyon
- Wolff AC, Hammond ME, Hicks DG et al (2013) Recommendations for human epidermal growth factor receptor 2 testing in breast cancer: American Society of Clinical Oncology/College of American Pathologists clinical practice guideline update. *J Clin Oncol* 31:3997–4013. <https://doi.org/10.1200/JCO.2013.50.9984>
- Pinker K, Bickel H, Helbich TH et al (2013) Combined contrast-enhanced magnetic resonance and diffusion-weighted imaging reading adapted to the “Breast Imaging Reporting and Data System” for multiparametric 3-T imaging of breast lesions. *Eur Radiol* 23:1791–1802. <https://doi.org/10.1007/s00330-013-2771-8>
- Fardanesh R, Marino MA, Avendano D, Leithner D, Pinker K, Thakur SB (2019) Proton MR spectroscopy in the breast: technical innovations and clinical applications. *J Magn Reson Imaging* 50:1033–1046. <https://doi.org/10.1002/jmri.26700>
- Galati F, Luciani ML, Caramanico C, Moffa G, Catalano C, Pediconi F (2019) Breast magnetic resonance spectroscopy at 3 T in biopsy-proven breast cancers: does choline peak correlate with prognostic factors? *Invest Radiol* 54:767–773. <https://doi.org/10.1097/RLI.0000000000000597>
- Choi JS, Baek HM, Kim S et al (2012) HR-MAS MR spectroscopy of breast cancer tissue obtained with core needle biopsy: correlation with prognostic factors. *PLoS One* 7:e51712. <https://doi.org/10.1371/journal.pone.0051712>
- Shin HJ, Baek HM, Cha JH, Kim HH (2012) Evaluation of breast cancer using proton MR spectroscopy: total choline peak integral and signal-to-noise ratio as prognostic indicators. *AJR Am J Roentgenol* 198:W488–W497. <https://doi.org/10.2214/AJR.11.7292>
- Chen JH, Mehta RS, Baek HM et al (2011) Clinical characteristics and biomarkers of breast cancer associated with choline concentration measured by 1H MRS. *NMR Biomed* 24:316–324. <https://doi.org/10.1002/nbm.1595>
- Baltzer PA, Dietzel M (2013) Breast lesions: diagnosis by using proton MR spectroscopy at 1.5 and 3.0 T—systematic review and meta-analysis. *Radiology* 267:735–746. <https://doi.org/10.1148/radiol.13121856>
- Types of breast cancer and related conditions. Available online: <https://www.cancerresearchuk.org/about-cancer/breast-cancer/stages-types-grades/types> (accessed on 1 June 2021)
- Thomas M, Kelly ED, Abraham J, Kruse M (2019) Invasive lobular breast cancer: a review of pathogenesis, diagnosis, management, and future

- directions of early stage disease. *Semin Oncol* 46:121–132. <https://doi.org/10.1053/j.seminoncol.2019.03.002>
33. McCart Reed AE, Kutasovic JR, Lakhani SR, Simpson PT (2015) Invasive lobular carcinoma of the breast: morphology, biomarkers and 'omics. *Breast Cancer Res* 17:12. <https://doi.org/10.1186/s13058-015-0519-x>
  34. Greenwood HI, Wilmes LJ, Kelil T, Joe BN (2020) Role of breast MRI in the evaluation and detection of DCIS: opportunities and challenges. *J Magn Reson Imaging* 52:697–709. <https://doi.org/10.1002/jmri.26985>
  35. Groen EJ, Elshof LE, Visser LL et al (2017) Finding the balance between over- and under-treatment of ductal carcinoma in situ (DCIS). *Breast* 31:274–283. <https://doi.org/10.1016/j.breast.2016.09.001>
  36. Salvatorelli L, Puzzo L, Vecchio GM, Caltabiano R, Virzi V, Magro G (2020) Ductal carcinoma in situ of the breast: an update with emphasis on radiological and morphological features as predictive prognostic factors. *Cancers (Basel)* 12:609. <https://doi.org/10.3390/cancers12030609>
  37. Tajima CC, de Sousa LLC, Venys GL, Guatelli CS, Bitencourt AGV, Marques EF (2019) Magnetic resonance imaging of the breast: role in the evaluation of ductal carcinoma in situ. *Radiol Bras* 52:43–47. <https://doi.org/10.1590/0100-3984.2018.0058>
  38. Greenwood HI, Heller SL, Kim S, Sigmund EE, Shaylor SD, Moy L (2013) Ductal carcinoma in situ of the breasts: review of MR imaging features. *Radiographics* 33:1569–1588. <https://doi.org/10.1148/rg.336125055>
  39. Mossa-Basha M, Fundaro GM, Shah BA, Ali S, Pantelic MV (2010) Ductal carcinoma in situ of the breast: MR imaging findings with histopathologic correlation. *Radiographics* 30:1673–1687. <https://doi.org/10.1148/rg.306105510>
  40. Kumar P, Aggarwal R (2016) An overview of triple-negative breast cancer. *Arch Gynecol Obstet* 293:247–269. <https://doi.org/10.1007/s00404-015-3859-y>
  41. Howlader N, Altekruse SF, Li CI et al (2014) US incidence of breast cancer subtypes defined by joint hormone receptor and HER2 status. *J Natl Cancer Inst* 106:dju055. <https://doi.org/10.1093/jnci/dju055>
  42. Richards CH, Mohammed Z, Qayyum T, Horgan PG, McMillan DC (2011) The prognostic value of histological tumor necrosis in solid organ malignant disease: a systematic review. *Future Oncol* 7:1223–1235. <https://doi.org/10.2217/fon.11.99>
  43. Cheon H, Kim HJ, Kim TH et al (2018) Invasive breast cancer: prognostic value of peritumoral edema identified at preoperative MR imaging. *Radiology* 287:68–75. <https://doi.org/10.1148/radiol.2017171157>
  44. Song SE, Shin SU, Moon HG, Ryu HS, Kim K, Moon WK (2017) MR imaging features associated with distant metastasis-free survival of patients with invasive breast cancer: a case-control study. *Breast Cancer Res Treat* 162:559–569. <https://doi.org/10.1007/s10549-017-4143-6>
  45. Net JM, Whitman GJ, Morris E et al (2019) Relationships between human-extracted MRI tumor phenotypes of breast cancer and clinical prognostic indicators including receptor status and molecular subtype. *Curr Probl Diagn Radiol* 48:467–472. <https://doi.org/10.1067/j.cpradiol.2018.08.003>
  46. Trop I, LeBlanc SM, David J et al (2014) Molecular classification of infiltrating breast cancer: toward personalized therapy. *Radiographics* 34:1178–1195. <https://doi.org/10.1148/rg.345130049>
  47. Tian L, Wang L, Qin Y (2020) Cai J (2020) Systematic review and meta-analysis of the malignant ultrasound features of triple negative breast cancer. *J Ultrasound Med* 39:2013–2025. <https://doi.org/10.1002/jum.15309>
  48. Boisserie-Lacroix M, Mac Grogan G, Debled M et al (2012) Radiological features of triple-negative breast cancers (73 cases). *Diagn Interv Imaging* 93:183–190. <https://doi.org/10.1016/j.diii.2012.01.006>
  49. Dogan BE, Turnbull LW (2012) Imaging of triple-negative breast cancer. *Ann Oncol* 23:23–29. <https://doi.org/10.1093/annonc/mds191>
  50. Öztürk VS, Polat YD, Soyder A, Tanyeri A, Karaman CZ, Taşkın F (2020) The relationship between MRI findings and molecular subtypes in women with breast cancer. *Curr Probl Diagn Radiol* 49:417–421. <https://doi.org/10.1067/j.cpradiol.2019.07.003>
  51. Wu M, Ma J (2017) Association between imaging characteristics and different molecular subtypes of breast cancer. *Acad Radiol* 24:426–434. <https://doi.org/10.1016/j.acra.2016.11.012>
  52. Kato F, Kudo K, Yamashita H et al (2016) Differences in morphological features and minimum apparent diffusion coefficient values among breast cancer subtypes using 3-Tesla MRI. *Eur J Radiol* 85:96–102. <https://doi.org/10.1016/j.ejrad.2015.10.018>
  53. Sung JS, Jochelson MS, Brennan S et al (2013) MR imaging features of triple-negative breast cancers. *Breast J* 19:643–649. <https://doi.org/10.1111/tbj.12182>
  54. Uematsu T (2011) MR imaging of triple-negative breast cancer. *Breast Cancer* 18:161–164. <https://doi.org/10.1007/s12282-010-0236-3>
  55. Lee YJ, Youn IK, Kim SH, Kang BJ, Park WC, Lee A (2020) Triple-negative breast cancer: pretreatment magnetic resonance imaging features and clinicopathological factors associated with recurrence. *Magn Reson Imaging* 66:36–41. <https://doi.org/10.1016/j.mri.2019.10.001>
  56. Agrawal G, Su MY, Nalcioğlu O, Feig SA, Chen JH (2009) Significance of breast lesion descriptors in the ACR BI-RADS MRI lexicon. *Cancer* 115:1363–1380. <https://doi.org/10.1002/cncr.24156>

## Publisher's Note

Springer Nature remains neutral with regard to jurisdictional claims in published maps and institutional affiliations.

**Submit your manuscript to a SpringerOpen® journal and benefit from:**

- Convenient online submission
- Rigorous peer review
- Open access: articles freely available online
- High visibility within the field
- Retaining the copyright to your article

Submit your next manuscript at ► [springeropen.com](https://www.springeropen.com)